 doi: 10.1111/j.1365-246X.2004.02511.x

FAST TRACK PAPER

Estimate of differential stress in the upper crust from variations in topography and strike along the San Andreas fault

Yuri Fialko,[1] Luis Rivera[2] and Hiroo Kanamori[3]

[1] *Institute of Geophysics and Planetary Physics, Scripps Institution of Oceanography, University of California San Diego, La Jolla,* CA 92093, *USA. E-mail: fialko@radar.ucsd.edu*

[2] *Ecole et Observatoire de Sciences de la Terre, Universite Louis Pasteur-CNRS, Strasbourg, France. E-mail: luis@sismo.u-strasbg.fr*

[3] *Seismological Laboratory, California Institute of Technology, Pasadena,* CA 91125, *USA. E-mail: hiroo@caltech.edu*

Accepted 2004 October 15; Received 2004 September 15; in original form 2004 April 21

SUMMARY

The major bends of the San Andreas fault in California are associated with significant variations in the along-fault topography. The topography-induced perturbations in the intermediate principal stress may result in the rotation of the fault with respect to the maximum compression axis provided that the fault is non-vertical, and the slip is horizontal. The progressive fault rotation may produce additional topography via thrust faulting in the adjacent crust, resulting in a positive feedback. The observed rotation of the fault plane due to the along-fault variations in topography is used to infer the magnitude of the in situ differential stress. Our results suggest that the average differential stress in the upper crust around the San Andreas fault is of the order of 50 MPa, implying that the effective fault strength is about a factor of two lower than predictions based on Byerlee's law and the assumption of hydrostatic pore pressure.

Key words: crustal deformation, fault tectonics, rock fracture, San Andreas fault, seismotectonics, transform faults.

1 INTRODUCTION

The San Andreas fault (SAF) in California is a prime example of a mature transform plate boundary in a continental setting. The 500-km long SAF exhibits several spectacular deviations from planarity (such as the Big Bend north of Los Angeles, Fig. 1), which are associated with variations in local topography. The observed correlation between the fault bends and topography is usually explained in terms of the kinematics of a long-term fault motion: the restraining fault bends result in a local compression, and 'push-up' thrust faulting, while the releasing bends produce extension, and 'pull-apart' normal faulting (Twiss & Moore 1992; Davis & Reynolds 1996). However, the relationships between the fault geometry, topography, and state of stress in the brittle crust have not been explicitly considered. In this paper we investigate the dynamics of a long-term slip on non-optimally oriented faults in the presence of variations in the along-fault topography. We use geological and seismological constraints on the present-day configuration of the SAF in the areas of major fault bends to derive a relationship between an increase in the vertical stress due to an excess topography, and the fault curvature. Our model is then used to estimate the magnitude of average differential stress in the brittle crust around the SAF.

2 DATA AND THEORY

The topography around the Big Bend and the San Bernardino segments of the SAF is shown in Figs 2(a) and (c), respectively. As can be seen from Fig. 2, there is a significant correlation between the fault strike and local topography. The fault rotates by about 20°–30° where it passes through an elevated terrain. We propose that this rotation is consistent with the topography-induced increase in vertical stress at the seismogenic depth, and may be used to infer the magnitude of the regional differential stress.

According to the Mohr–Coulomb theory, shear failure in a homogeneous medium subject to a uniform triaxial stress should occur on optimally oriented planes (i.e. planes containing the intermediate principal stress axis, and oriented at an acute angle to the maximum compressive stress axis) (Anderson 1951; Scholz 1990; King *et al.* 1994). Failure occurs when the differential stress $\sigma_1 - \sigma_3$, where σ_1 and σ_3 are the maximum and minimum compressive stresses, respectively, reaches a critical value of the order of the effective normal stress (normal stress minus the pore pressure) (Byerlee 1978). The Mohr–Coulomb failure criterion is intrinsically 2-D, and independent of the value of the intermediate stress σ_2. Assuming that the intermediate stress axis is oriented vertically, as appropriate for strike-slip faulting (Anderson 1951), the Mohr–Coulomb theory

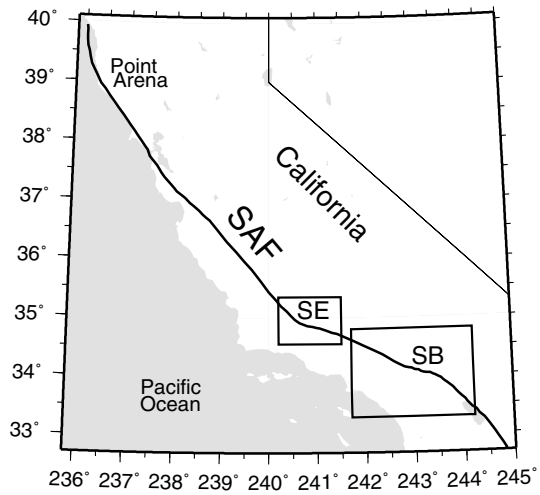

Figure 1. Map showing the geometry of the San Andreas fault (SAF, thick wavy line) in California. Rectangular boxes outline the major fault bends (SE—San Emigdio bend ('Big Bend'), SB—San Bernardino bend).

predicts horizontal slip on vertical planes, regardless of variations in the intermediate stress. There is evidence, however, that the SAF may not be optimally oriented for failure along much of its length (Zoback *et al.* 1987; Mount & Suppe 1987; Nur *et al.* 1993), and, furthermore, may have a non-vertical dip angle within the major fault bends while keeping an essentially horizontal slip direction (Nicholson *et al.* 1986; Griscom & Jachens 1990; Seeber & Armbruster 1995). If so, the mechanics of slip on non-optimally oriented surfaces may be explicitly dependent on the intermediate stress σ_2. Slip on a non-optimally oriented surface may occur, for example if the work required to generate a new fault is greater than the work against friction on a pre-existing surface.

Consider an arbitrarily oriented fault plane defined by a unit normal n_i ($i = 1, 2, 3$) in a coordinate system x_i associated with the principal stresses ($\sigma_1, \sigma_2, \sigma_3$) (Fig. 3). Hereafter, the intermediate stress σ_2 is assumed to be vertical. Components of the unit vector n_i satisfy the following identity:

$$n_i n_i = n_1^2 + n_2^2 + n_3^2 = 1 \tag{1}$$

(as usual, the repeating indexes imply summation). Let τ_{ij} be the stress tensor, such that in the principal stress coordinate system

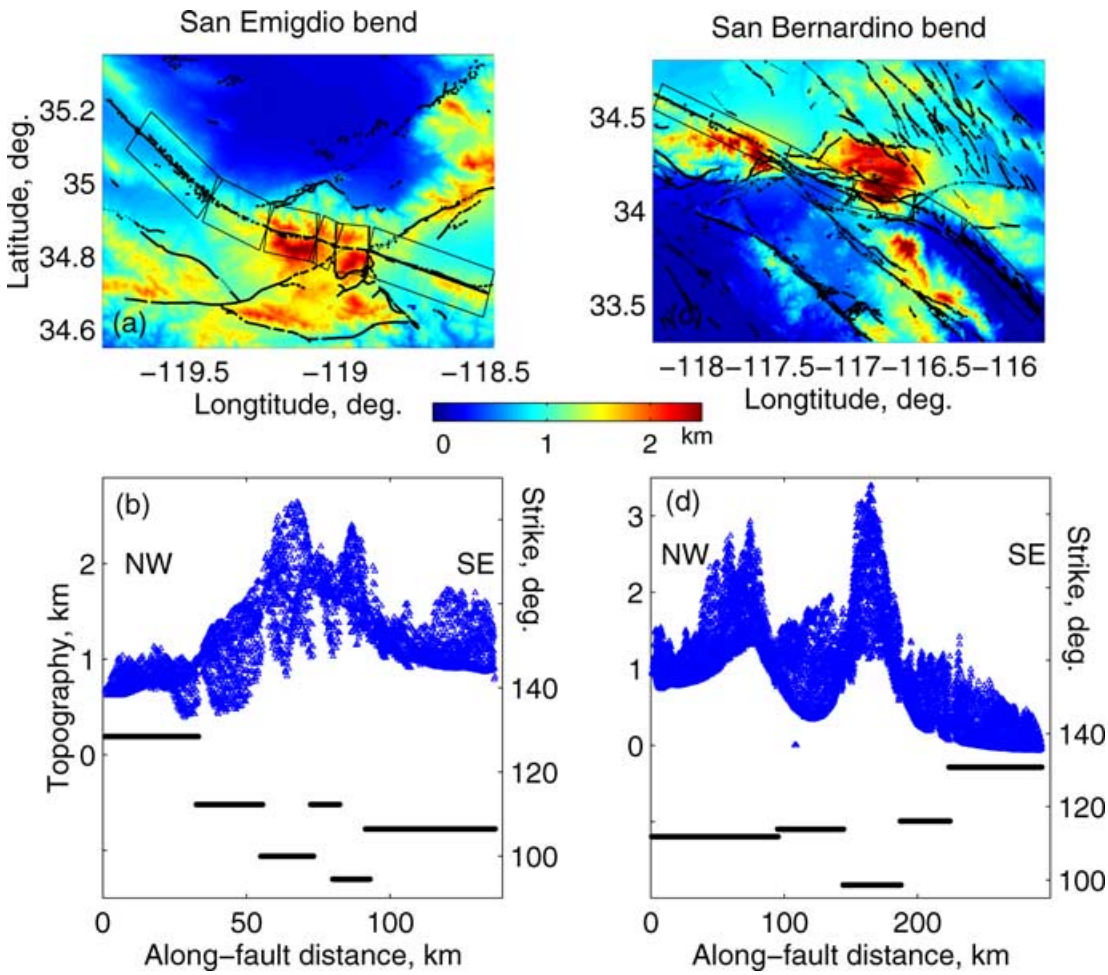

Figure 2. Digital elevation map (Farr & Kobrick 2000) of areas adjacent to the SAF near (a) the Big Bend (San Emigdio bend), and (c) the San Bernardino bend. Figs (b) and (d) show the along-fault variations in topography (triangles) and fault strike (solid lines). Topography data represent elevation above sea level taken from 10-km wide swathes centred on the fault trace (rectangular boxes in parts a and c). The local fault strike is measured clockwise from the north using the same fault discretization as shown in parts a and c.

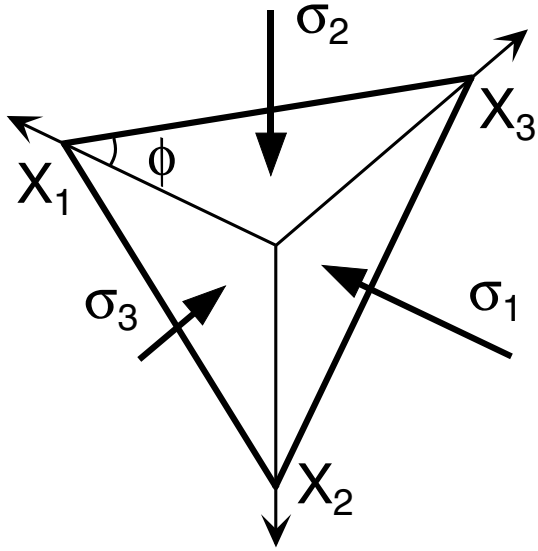

Figure 3. An arbitrarily oriented fault plane subject to the tri-axial stress field ($\sigma_1, \sigma_2, \sigma_3$).

(Fig. 3) $\tau_{11} = \sigma_1$, $\tau_{22} = \sigma_2$, $\tau_{33} = \sigma_3$, and the non-diagonal components of τ_{ij} are zeros. The total traction F_i acting on the fault surface is

$$F_i = \tau_{ij} n_j = \begin{cases} \sigma_1 n_1 \\ \sigma_2 n_2 \\ \sigma_3 n_3 \end{cases} \tag{2}$$

The normal stress τ_n and the shear stress τ_t resolved on the fault surface are

$$\tau_n = \tau_{ij} n_j n_i = \sigma_1 n_1^2 + \sigma_2 n_2^2 + \sigma_3 n_3^2, \tag{3}$$

$$\tau_t = \tau_{ij} n_j t_i. \tag{4}$$

In eq. (4), t_i is the unit vector denoting a direction in which the shear stress τ_t is resolved on a fault plane. For a given stress state, the maximum shear traction $\tau^m{}_t$ acting on a fault plane depends on the fault orientation only:

$$\tau_t^m t_i^m = F_i - \tau_n n_i = \begin{cases} (\sigma_1 - \tau_n) n_1 \\ (\sigma_2 - \tau_n) n_2 \\ (\sigma_3 - \tau_n) n_3 \end{cases} \tag{5}$$

where $t^m{}_i$ is the direction in which τ_t^m is acting. Analogous expressions for the normal and shear stresses resolved on a fault plane can be found by considering a 3-D Mohr circle diagram (Jaeger 1956). Eqs (3) and (5) indicate that for vertical faults ($n_2 = 0$) both the normal and the maximum shear stresses (and thus the Mohr–Coulomb failure criterion) are independent of the intermediate stress σ_2, as expected. We are interested in the dynamics of slip on a fault plane that may not be optimally oriented for failure, and is not collinear with any of the principal stress axes. It is reasonable to assume that the long-term slip on mature faults occurs in the direction of the maximum shear tractions t_i^m. This assumption is similar to those used in, for example, inversions of the fault slip or the earthquake focal mechanism data for the principal stress orientations (Gephart & Forsyth 1984; Rivera & Cisternas 1990; Hardebeck & Hauksson 1999). Eq. (5) indicates that for non-vertical faults ($n_2 \neq 0$) the condition of pure strike-slip ($t_2^m = 0$) can be satisfied if and only if the vertical stress equals the normal stress resolved on the fault plane:

$$\tau_n = \sigma_2. \tag{6}$$

Condition (6) can be exploited to establish a relationship between variations in the vertical stress σ_2 (e.g. due to topography), and the associated variations in the fault orientation n_i that render the equilibrium values of the fault-normal stress τ_n. Eliminating an explicit dependence of the normal stress on n_3 using constraint (1), $n_3^2 = 1 - n_1^2 - n_2^2$, from eqs (3) and (6) one obtains

$$\sigma_2 - \sigma_3 - (\sigma_1 - \sigma_3) n_1^2 - (\sigma_2 - \sigma_3) n_2^2 = 0. \tag{7}$$

The relationship (7) admits separation of terms that depend only on the state of stress (σ_i) and the fault orientation (n_i):

$$\frac{\sigma_2 - \sigma_3}{\sigma_1 - \sigma_3} = \frac{n_1^2}{1 - n_2^2}. \tag{8}$$

The left-hand side of eq. (8) is a well-known stress ratio R that characterizes the shape of the stress ellipsoid (Bott 1959; Rivera & Cisternas 1990). The right-hand side of eq. (8) can be re-written in terms of the direction cosines n_1 and n_3 only (e.g. using relationship 1):

$$\frac{n_1^2}{1 - n_2^2} = \frac{1}{1 + (n_3/n_1)^2}. \tag{9}$$

Noting that the ratio n_3/n_1 represents a cotangent of the angle ϕ between the fault trace and the σ_1 axis (i.e. the fault 'strike' in the principal coordinate system, positive counter-clockwise, Fig. 3), and using the trigonometric identity $(1 + \cot^2\phi)^{-1} = \sin^2\phi$, from eqs (8) and (9) one obtains the following relationship between the stress ratio and the fault orientation:

$$\frac{\sigma_2 - \sigma_3}{\sigma_1 - \sigma_3} = \sin^2 \phi. \tag{10}$$

Note that for non-vertical strike-slip faults the relationship (10) must be satisfied regardless of the fault dip angle.

Provided that the horizontal stress is homogeneous, eq. (10) predicts that an increase in the intermediate stress σ_2 (e.g. due to an excess topography) should cause an increase in the angle ϕ, i.e. a rotation of a fault in the horizontal plane away from the σ_1 axis. Conversely, a decrease in σ_2 should cause a fault rotation towards the σ_1 axis. These predictions are consistent with the observed variations in topography and fault strike along the SAF (Fig. 1), and the approximately NNE orientation of the maximum compression axis in California (Lisowski *et al.* 1991; Unruh *et al.* 1996). In particular, the SAF rotates counter-clockwise where it crosses the mountains (Big Bend and San Bernardino areas), and clockwise where it drops below the sea level (e.g. north of Point Arena and around the Salton Sea, see Fig. 1). Predictions of eq. (10) admit a simple physical interpretation. An increase in the vertical stress on a dipping fault introduces a component of normal faulting into the resolved shear stress on the fault. In order to maintain the strike-slip, the fault must rotate to higher angles to the maximum compressive stress axis, thereby introducing a component of thrust faulting that will balance out the component of normal faulting introduced by the excess topography.

The topography-induced perturbations in the intermediate stress in the upper crust may be readily estimated given the 'excess' topography Δh: $\Delta\sigma_2 = \rho_r g \Delta h$, where ρ_r is the rock density, and g is the gravitational acceleration. Because the amount of the topography-induced fault rotation necessarily depends on the average differential stress $\sigma_1 - \sigma_3$ in the brittle layer, the latter may be determined from

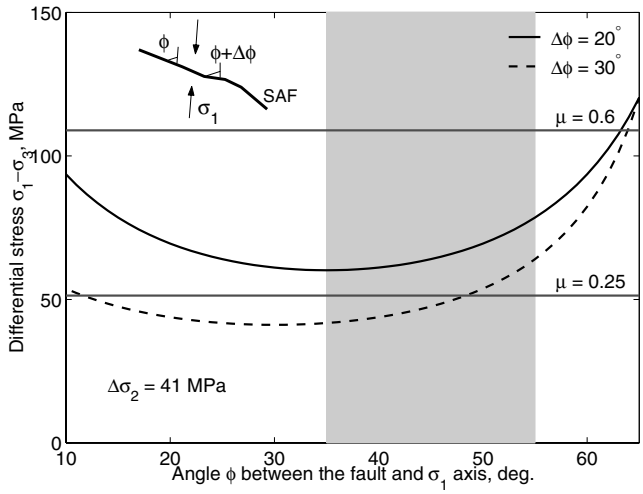

Figure 4. Dependence of the differential stress on the angle ϕ between the fault and the maximum compressive stress axis, for values of $\Delta\phi$ spanning the likely range of the observed fault rotation. The shaded area indicates the range of ϕ inferred from the inversions of the earthquake focal mechanisms (Hardebeck & Hauksson 1999). Horizontal lines show the maximum average differential stress for various coefficients of friction μ. The inset illustrates the geometry of the problem.

eq. (10) by relating the estimated changes in the vertical stress $\Delta\sigma_2$ to the observed changes in the fault strike $\Delta\phi$:

$$\sigma_1 - \sigma_3 = \frac{2\Delta\sigma_2}{\cos 2\phi - \cos 2(\phi + \Delta\phi)}. \tag{11}$$

Fig. 4 shows the average differential stress calculated using eq. (11) for a range of possible values of the angle ϕ between the fault trace and the maximum compression axis, and the fault rotation $\Delta\phi$ of 20° to 30° suggested by the geological data (Figs 1 and 2). In our calculations we assume a rock density of 2.8×10^3 kg m^{-3}, and average excess elevation of 1.5 km along the major bends of the SAF (Fig. 2). For comparison, we also show the maximum average differential stress in the brittle layer predicted by Mohr–Coulomb theory under the assumption of hydrostatic pore pressure:

$$\Delta\sigma_{\max} = \frac{1}{H}\int_0^H (\sigma_1 - \sigma_3)\, dz = \frac{(\rho_r - \rho_w) g H \mu}{\sqrt{1+\mu^2}}, \tag{12}$$

where ρ_w is the water density, H is the thickness of the brittle layer, and μ is the coefficient of friction (see horizontal lines in Fig. 1) (Byerlee 1978; Townend & Zoback 2000).

3 DISCUSSION

There is a long-standing debate in earthquake physics regarding the magnitude of shear stresses on average supported by major seismogenic faults in the Earth's crust (Scholz 1990; Rice 1992; Zoback *et al.* 1993). The empirical Mohr–Coulomb failure theory, based on a large number of rock fracture experiments, predicts that faults slip when shear stresses in the host rocks are of the order of the lithostatic stress, provided that the pore fluid pressure does not significantly exceed hydrostatic (Anderson 1951; Byerlee 1978). Assuming a typical depth of the seismogenic zone of 12 km, a rock density of 2.8×10^3 kg m^{-3}, and a coefficient of friction of 0.6, the fault-averaged shear stress on the verge of failure is of the order of 10^8 Pa. Measurements in deep boreholes seem to indicate that stresses in the upper crust in general obey Byerlee friction, and, moreover, the state of stress in the crust is near the failure envelope even in areas that are not tectonically or seismically active (Townend & Zoback 2000). On the other hand, typical earthquake stress drops of the order of 10^6–10^7 Pa (Kanamori & Anderson 1975), the common absence of melting on localized fault slip zones (Chester & Chester 1998), the lack of a significant heat flow anomaly (Lachenbruch & Sass 1980), and the nearly orthogonal orientation of the far-field principal compression axis to the SAF (Mount & Suppe 1987) have been used to argue that large crustal faults may operate at relatively low driving stresses of the order of a few tens of megapascals or less. The latter statement constitutes the 'weak fault' hypothesis (Rice 1992). Given the geological and seismological constraints on the contemporaneous kinematics of the SAF, the along-fault variations in strike and topography described in the previous section can be used to provide an independent estimate on the level of the in situ deviatoric stress in the crust around the SAF.

A robust inference of the average differential stress from eq. (11) requires knowledge of the orientation of the maximum principal stress σ_1 (i.e. the angle ϕ). Assuming that the regional crustal stress is relatively homogeneous on a spatial scale of the order of the wavelength of the major fault bends (i.e. tens of kilometres), a lower bound on ϕ is given by the condition that the rotated section of the fault must have the same sense of shear stress as the rest of the fault, implying $\phi < \pi/2 - \Delta\phi$. The precise values of ϕ are the subject of a significant debate. Several lines of evidence, including inversions of seismic focal mechanisms, measurements of the long-term geodetic strain, borehole data, and structural geological mapping around the SAF suggest that the regional σ_1 axis may be oriented at high angles (60°–80°) to the SAF (Mount & Suppe 1987; Lisowski *et al.* 1991; Zoback *et al.* 1993). Other interpretations of similar data favour values of ϕ scattered around 45° (McNally *et al.* 1978; Zoback *et al.* 1980). Hardebeck & Hauksson (1999) proposed that the σ_1 axis rotates to intermediate (35°–55°) angles within a few tens of kilometres from the fault, based on inversions of a number of the earthquake focal mechanisms (see shaded area in Fig. 4). Their data also show that the orientation of the σ_1 axis is approximately constant around the San Bernardino bend, consistent with our assumption of a locally homogeneous stress field. As one can see from Fig. 4, for the intermediate values of angles ϕ obtained by Hardebeck & Hauksson (1999) our model gives rise to differential stresses of 40–60 MPa, or fault-averaged shear stresses of the order of 20–30 MPa. The inferred stresses are about two to three times lower than those predicted assuming the laboratory values of the coefficient of friction ($\mu = 0.6$–0.8) and hydrostatic pore pressures (see eq. 11 and Fig. 4), but are on the high end of constraints provided by the heat flow measurements (Brune *et al.* 1969; Lachenbruch & Sass 1980). These results suggest that the strength of the SAF falls between the predictions of the strong (Scholz 2000) and weak (Rice 1992) fault theories. Recently, Townend & Zoback (2004) analysed an earthquake data set similar to that used by Hardebeck & Hauksson (1999), and concluded that the angle between the maximum compressive stress axis and the SAF in southern California is about 60°–70°. Taken at face value, this inference might be interpreted as indicating the high strength of the SAF (Fig. 4). However, the interpretation of Townend & Zoback (2004) implies that the orientation of the σ_1 axis correlates with the local fault strike. If so, our assumption of the locally homogeneous horizontal stress field is invalid, and eq. (10) cannot be used to deduce the magnitude of the differential stress.

In addition to the assumption of the homogeneous stress state, our estimate of the in situ differential stress relies on the assumption of horizontal slip on a non-vertical fault. The evidence for a

dipping geometry of the SAF around the San Emigdio, San Bernardino, and Point Arena bends includes seismic, magnetic, gravity, and geological observations (McNally *et al.* 1978; Nicholson *et al.* 1986; Griscom & Jachens 1990; Seeber & Armbruster 1995; Magistrale & Sanders 1996; Yule & Sieh 2003), although details of the SAF configuration beneath the major bends are still debated (Carena *et al.* 2004). While the non-vertical fault orientation may initially develop in response to a transpressional or transtensional stress regime, thereby allowing the fault to accommodate some fault-normal displacements, the seismic and geomorhological data suggest that the current kinematics of the SAF within the fault bends is predominantly strike-slip, and that most of the convergence/extension across the bends is taken up by the thrust/normal faulting in the ambient crust (Twiss & Moore 1992; Davis & Reynolds 1996; Yule & Sieh 2003). The partitioning of oblique convergence onto the purely strike-slip and dip-slip fault systems is well known and has been previously explained in terms of the least-work principle (Michael 1990). However, to date no mechanical energy calculations exist for the case of non-planar faults, and it remains to be seen whether the least-work principle can explain the observed geometry of the SAF. We note that the topography-induced fault rotation required to preserve the strike-slip setting decreases shear stress, and increases normal stress on the fault plane, moving it further from the failure envelope. Therefore the long-term persistence of the major fault bends implies either that the bends are weaker compared with the rest of the fault, or that the bend geometry minimizes the total work (including the mechanical energy, as well as changes in the gravitational potential energy) spent on slip on the SAF and the adjacent faults in the presence of the along-strike variations in topography. Because the total work done against the fault friction depends on the depth-averaged normal stress within the brittle layer, our model implies that the depth to the brittle–ductile transition does not track the surface topography. The seismic data (in particular, the hypocentral depths of local earthquakes) do not indicate any shallowing of the brittle–ductile transition beneath the major fault bends (Hill *et al.* 1990; Richards-Dinger & Shearer 2000), lending support to our model assumptions.

We point out that our analysis may be relevant for long-term slip on faults with large total offsets. Individual earthquakes and young faults may exhibit significant deviations from the suggested relationship between the topography and the fault geometry. For example, the surface rupture of the 1999 Hector Mine earthquake in southern California changes its strike where it crosses the relatively small (average elevation of $\sim$0.5 km) Bullion mountains (USGS *et al.* 2000; Fialko *et al.* 2001). The sense of the rupture rotation, however, is opposite to that predicted by eq. (10). Time-dependent inversions of seismic data (Ji *et al.* 2002) indicate that the Hector Mine rupture initiated on a central segment of the fault that may have been more optimally oriented for failure, and then propagated bi-laterally on pre-existing faults that are at a higher angle with respect to the regional compression axis (Nur *et al.* 1993). Therefore the along-fault variations in strike in the case of the Hector Mine earthquake may be due to the heterogeneous strength of the crust and the dynamic aspects of the rupture, rather than to the long-term effects of topography considered in this paper.

As the along-strike variations in topography affect the fault geometry only insofar as they affect the shear stress resolved on the fault plane, the vertical segments of strike-slip faults should not exhibit any correlation between the local topography and the fault strike. A possible example may be a stretch of the SAF north of the San Bernardino bend (Fig. 2c). This part of the SAF is believed to have a near-vertical dip throughout the brittle layer (Griscom & Jachens 1990), and it does not exhibit any appreciable deviations from planarity where it passes through an elevated terrain (Figs 2c and d). While the particular mechanisms leading to the development of major fault bends remain poorly understood, our model suggests that a relationship between the topographically induced perturbation in the intermediate principal stress, and changes in the fault strike for non-vertical faults may result in a positive feedback mechanism, whereby a build-up in elevation due to thrust faulting around a compressive bend is likely to cause a further rotation of the fault. The long-lived fault bends may therefore represent a stable configuration corresponding to either the reduced effective coefficient of friction within the bent fault section, or the minimum energy dissipation on the entire fault system including the main strike-slip fault, as well as the associated dip-slip faults in the ambient crust. Alternatively, a continued build-up of topography by thrust faulting may result in a complete locking of the fault bend, and a subsequent reorganization of the fault geometry. This may have a bearing on the observed branching of the SAF, for example in the vicinity of the San Bernardino segment (Fig. 2c), and the strain transfer from the SAF system to the Eastern California shear zone (Dokka & Travis 1990; Nur *et al.* 1993; Rockwell *et al.* 2000).

4 CONCLUSIONS

We combined the kinematic constraints on the configuration and long-term slip of the San Andreas fault with the dynamics of slip on an arbitrarily oriented surface to investigate the observed correlation between the major bends of the SAF in California and variations in the along-fault topography. We demonstrate that the topography-induced perturbations in the intermediate (vertical) principal stress may enhance bending of a non-optimally oriented fault due to an azimuthal rotation of the pure strike-slip vector. In the presence of the excess topography, the slip vector is predicted to rotate away from the maximum compression axis. The observed rotation of the fault plane due to variations in topography along the SAF is consistent with the model predictions. The fault rotation may result from either the progressive reduction in the effective coefficient of friction within the bent fault section, or the minimization of total work spent on slip on the main strike-slip fault, as well as on the associated dip-slip faults in the ambient crust. Regardless of the particular mechanism of the fault bending, the observed variations in the fault strike and topography may be used to infer the magnitude of the in situ differential stress provided that the following conditions are met: (1) the fault is non-vertical; (2) the long-term fault slip is horizontal; and (3) the horizontal stress state has little variability on the spatial scale of the order of the fault-bend wavelength. Several lines of geological and geophysical data indicate that these conditions are indeed satisfied around the major fault bends of the SAF. For the seismologically inferred angles between the average fault strike and the maximum compression axis in southern California of 35°–55° (Hardebeck & Hauksson 1999), our results suggest that the average differential stress in the upper crust is of the order of 50 MPa, implying that the effective strength of the San Andreas fault is about a factor of two lower compared with predictions based on Byerlee's law and the assumption of hydrostatic pore pressures, but is at the high end of constraints provided by heat flow measurements.

ACKNOWLEDGMENTS

We thank two anonymous reviewers and the Editor Cindy Ebinger for their insightful comments and suggestions. This material is based

upon work partially supported by the National Science Foundation under Grant EAR-0338061, and the Southern California Earthquake Center (SCEC). SCEC is funded by NSF Cooperative Agreement EAR-0106924 and USGS Cooperative Agreement 02HQAG0008. The SCEC contribution number for this paper is 806.

REFERENCES

Anderson, E.M., 1951. *The Dynamics of Faulting,* Oliver and Boyd, Edinburgh.

Bott, M., 1959. The mechanics of oblique slip faulting, *Geol. Mag.,* **96,** 109–117.

Brune, J.N., Henyey, T. & Roy, R., 1969. Heat flow, stress, and rate of slip along San Andreas fault, California, *J. geophys. Res.,* **74,** 3821–4009.

Byerlee, J., 1978. Friction of rock, *Pure appl. Geophys.,* **116,** 615–626.

Carena, S., Suppe, J. & Kao, H., 2004. Lack of continuity of the San Andreas Fault in southern California: Three-dimensional fault models and earthquake scenarios, *J. geophys. Res.,* **109,** doi:10.1029/2003JB002643.

Chester, F.M. & Chester, J.S., 1998. Ultracataclasite structure and friction processes of the Punchbowl fault, San Andreas system, California, *Tectonophysics,* **295,** 199–221.

Davis, G. & Reynolds, S., 1996. *Structural Geology of Rocks and Regions,* John Wiley and Sons, New York.

Dokka, R.K. & Travis, C.J., 1990. Role of the Eastern California shear zone in accommodating Pacific-North American plate motion, *Geophys. Res. Lett.,* **17,** 1323–1327.

Farr, T. & Kobrick, M., 2000. Shuttle Radar Topography Mission produces a wealth of data, *EOS, Trans. Am. geophys. Un.,* **81,** 583–585.

Fialko, Y., Simons, M. & Agnew, D., 2001. The complete (3-D) surface displacement field in the epicentral area of the 1999 M_w7.1 Hector Mine earthquake, southern California, from space geodetic observations, *Geophys. Res. Lett.,* **28,** 3063–3066.

Gephart, J.W. & Forsyth, D.W., 1984. An improved method for determining the regional stress tensor using earthquake focal mechanism data: Application to the San Fernando earthquake sequence, *J. geophys. Res.,* **89,** 9305–9320.

Griscom, A. & Jachens, R., 1990. Crustal and lithospheric structure from gravity and magnetic studies, in *The San Andreas Fault System, California, USGS Open Prof. Pap. 1515,* pp. 239–259, ed. Wallace, R., US Government Printing Office, Washington, DC.

Hardebeck, J.L. & Hauksson, E., 1999. Role of fluids in faulting inferred from stress field signatures, *Science,* **285,** 236–239.

Hill, D., Eaton, J. & Jones, L., 1990. Seismicity, 1980-86, in *The San Andreas Fault System, California, USGS Open Prof. Pap. 1515,* pp. 115–152, ed. Wallace, R., US Government Printing Office, Washington, DC.

Jaeger, J., 1956. *Elasticity, Fracture, and Flow,* John Wiley, New York.

Ji, C., Wald, D. & Helmberger, D., 2002. Source description of the 1999 Hector Mine, California, earthquake, part II: Complexity of slip history, *Bull. seism. Soc. Am.,* **92,** 1208–1226.

Kanamori, H. & Anderson, D.L., 1975. Theoretical basis of some empirical relations in seismology, *Bull. seism. Soc. Am.,* **65,** 1073–1095.

King, G.C.P., Stein, R.S. & Lin, J., 1994. Static stress changes and the triggering of earthquakes, *Bull. seism. Soc. Am.,* **84,** 935–953.

Lachenbruch, A.H. & Sass, J.H., 1980. Heat flow and energetics of the San Andreas fault zone, *J. geophys. Res.,* **85,** 6185–6222.

Lisowski, M., Savage, J. & Prescott, W.H., 1991. The velocity field along the San Andreas fault in central and southern California, *J. geophys. Res.,* **96,** 8369–8389.

McNally, K., Kanamori, H., Pechmann, J. & Fuis, G., 1978. Earthquake swarm along the San Andreas fault near Palmdale, southern California, 1976 to 1977, *Science,* **201,** 814–817.

Magistrale, H. & Sanders, C., 1996. Evidence from precise earthquake hypocenters for segmentation of the San Andreas fault in San Gorgonio Pass, *J. geophys. Res.,* **101,** 3031–3044.

Michael, A., 1990. Energy constraints on kinematic models of oblique faulting—Loma-Prieta versus Parkfield-Coalinga, *Geophys. Res. Lett.,* **9,** 1453–1456.

Mount, V. & Suppe, J., 1987. State of stress near the San Andreas fault: Implications for wrench tectonics, *Geology,* **15,** 1143–1146.

Nicholson, C., Seeber, L. & Williams, P., 1986. Seismicity and fault kinematics through the eastern Transverse ranges, California—block rotation, strike-slip faulting and low-angle thrusts, *J. geophys. Res.,* **91,** 4891–4908.

Nur, A., Ron, H. & Beroza, G., 1993. The nature of the Landers-Mojave earthquake line, *Science,* **261,** 201–203.

Rice, J.R., 1992. Fault stress states, pore pressure distribution, and the weakness of the San Andreas Fault, in *Fault Mechanics and Transport Properties of Rocks,* pp. 475–503, eds Evans, B. & Wong, T., Academic, San Diego.

Richards-Dinger, K. & Shearer, P., 2000. Earthquake locations in southern California obtained using source specific station terms, *J. geophys. Res.,* **105,** 10 939–10 960.

Rivera, L. & Cisternas, A., 1990. Stress tensor and fault plane solutions for a population of earthquakes, *Bull. seism. Soc. Am.,* **80,** 600–614.

Rockwell, T., Lindvall, S., Herzberg, M., Murbach, D., Dawson, T. & Berger, G., 2000. Paleoseismology of the Johnson Valley, Kickapoo, and Homestead Valley faults: Clustering of earthquakes in the eastern California shear zone, *Bull. seism. Soc. Am.,* **90,** 1200–1236.

Scholz, C.H., 1990. *The Mechanics of Earthquakes and Faulting,* Cambidge Univ. Press, New York.

Scholz, C., 2000. Evidence for a strong San Andreas fault, *Geology,* **28,** 163–166.

Seeber, L. & Armbruster, J., 1995. The San-Andreas fault system through the Transverse ranges as illuminated by earthquakes, *J. geophys. Res.,* **100,** 8285–8310.

Townend, J. & Zoback, M., 2000. How faulting keeps the crust strong, *Geology,* **28,** 399–402.

Townend, J. & Zoback, M., 2004. Regional tectonic stress near the san andreas fault in central and southern california, *Geophys. Res. Lett.,* **31,** Art. No. L15S11, doi:10.1029/2003GL018918.

Twiss, R. & Moore, E., 1992. *Structural Geology,* W.H. Freeman, New York.

Unruh, J.R., Twiss, R.J. & Hauksson, E., 1996. Seismogenic deformation field in the Mojave block and implications for tectonics of the eastern California shear zone, *J. geophys. Res.,* **101,** 8335–8361.

USGS, SCEC & the California Division of Mines & Geology, 2000. Preliminary report on the 16 October 1999 M7.1 Hector Mine, California, earthquake, *Seism. Res. lett.,* **71,** 11–23.

Yule, D. & Sieh, K., 2003. Complexities of the San Andreas fault near San Gorgonio Pass: Implications for large earthquakes, *J. geophys. Res.,* **108,** doi:10.1029/2001JB000451.

Zoback, M., Tsukahara, H. & Hickman, S., 1980. Stress measurements at depth in the vicinity of the San Andreas fault: Implications for the magnitude of shear stress at depth, *J. geophys. Res.,* **85,** 6157–6173.

Zoback, M. *et al.,* 1987. New evidence on the state of stress of the San-Andreas fault system, *Science,* **238,** 1105–1111.

Zoback, M. *et al.,* 1993. Upper-crustal strength inferred from stress measurements to 6 km depth in the KTB borehole, *Nature,* **365,** 633–635.